


Article

Theoretical Insights into the Solvent Polarity Effect on the Quality of Self-Assembled *N*-Octadecanethiol Monolayers on Cu (111) Surfaces

Jun Hu ^{1,*} , Shijun He ¹, Yaozhong Zhang ², Haixia Ma ¹, Xiaoli Zhang ¹ and Zhong Chen ^{3,*}

¹ School of Chemical Engineering, Northwest University, Xi'an 710069, Shaanxi, China; heshijun0717@163.com (S.H.); mahx@nwu.edu.cn (H.M.); xlzhang@nwu.edu.cn (X.Z.)

² State Key Laboratory of Eco-Hydraulics in Northwest Arid Region of China, Xi'an University of Technology, Xi'an 710048, Shaanxi, China; zhangyz@xaut.edu.cn

³ School of Materials Science and Engineering, Nanyang Technological University, 50 Nanyang Avenue, Singapore 639798, Singapore

* Correspondence: hujun32456@163.com (J.H.); ASZChen@ntu.edu.sg (Z.C.); Tel.: +65-6790-4256 (Z.C.)

Received: 9 February 2018; Accepted: 21 March 2018; Published: 22 March 2018



Abstract: The effect of solvent polarity on the quality of self-assembled *n*-octadecanethiol (C₁₈SH) on Cu surfaces was systematically analyzed using first-principles calculations. The results indicate that the adsorption energy for C₁₈SH on a Cu surface is −3.37 eV, which is higher than the adsorption energies of the solvent molecules. The higher adsorption energy of dissociated C₁₈SH makes the monolayer self-assembly easier on a Cu (111) surface through competitive adsorption. Furthermore, the adsorption energy per unit area for C₁₈SH decreases from −3.24 eV·Å^{−2} to −3.37 eV·Å^{−2} in solvents with an increased dielectric constant of 1 to 78.54. Detailed energy analysis reveals that the electrostatic energy gradually increases, while the kinetic energy decreases with increasing dielectric constant. The increased electrostatic energies are mainly attributable to the disappearance of electrostatic interactions on the sulfur end of C₁₈SH. The decreased kinetic energy is mainly due to the generated push force in the polar solvent, which limits the mobility of C₁₈SH. A molecular dynamics simulation also confirms that the −CH₃ site has a great interaction with CH₃(CH₂)₄CH₃ molecules and a weak interaction with CH₃CH₂OH molecules. The different types of interactions help to explain why the surface coverage of C₁₈SH on Cu in a high-polarity ethanol solution is significantly larger than that in a low-polarity *n*-hexane solution at the stabilized stage.

Keywords: copper; corrosion; density functional theory; solvent polarity; self-assembled monolayer

1. Introduction

Copper (Cu) and its alloys have been widely used in many industrial sectors, including electronic, chemical, and ocean engineering [1]. Despite its many outstanding properties, Cu is very chemically active, and is thus prone to corrosion. Serious corrosion not only leads to grave economic loss, it also poses a potential threat to human life [2–4]. Various ways to protect metals from corrosion have been developed based on different principles. Self-Assembled Monolayers (SAMs) are one of the most economic, highly efficient, and simple ways to protect metals and alloys from corrosion and oxidization [5–7]. Experimental research has been carried out to identify the protection mechanism of SAMs on Cu surfaces. It was generally believed that the densely packed monolayers were formed through chemisorption onto the surface of Cu [8]. Since the properties of the solvent affect the assembly of SAMs, the qualities of the SAMs formed in different solvents are expected to be different. Thus far, many researchers have studied the thiol-SAMs formed on gold surfaces in different solvents. Among them, Bain et al. evaluated the effect of various solvents (dimethylformamide, tetrahydropyranyl,

ethanol, carbon tetrachloride, acetonitrile, hexadecane, cyclooctane, and toluene) on the formation of SAMs on gold surfaces. It was found that the hexadecanethiol monolayer adsorbed on gold in a hexadecane solution displays a low contact angle when it reaches certain thickness, which can possibly be attributed to the incorporation of hexadecane into the monolayer [9]. Dai et al. have reported the effects of solvents on the quality of the SAM of dodecanethiol on gold. They revealed that the solvent parameters (such as polarity, solubility, molecular size, octanol-water partition coefficients, and viscosity) affect the quality of the C₁₂SH SAMs [10]. Ujjal et al. have also proposed that the nature of the solvent might affect the blocking properties and barrier characteristics of the –CH₃ terminated SAMs [11,12]. Our previous experiments by electrochemical impedance spectroscopy, Fourier transform infrared spectroscopy, and X-ray photoelectron spectroscopy, showed that the qualities of self-assembled *n*-octadecanethiol (C₁₈SH) indeed differ when it is formed in different solvents (*n*-hexane, toluene, trichloroethylene, chloroform, acetone, acetonitrile, and ethanol) [13]. Based on the experimental results, the assembly is likely to be a competitive adsorption process, containing interactions among the solvent, the solute, and the surface. However, which of these interactions plays an important role during the self-assembly process remains unclear due to the potential complexity of interactions among the different entities.

Computational analysis, on the other hand, is able to overcome the experimental limitations, and thus provides a very useful tool to understand the assembly mechanisms [14–17]. Benchouk et al. studied the effect of solvents on the 1,3-dipolar cycloaddition of benzonitrile *N*-oxide with cyclopentene using first-principles calculations. They found that solvent polarity leads to the slow inhibition of the 1,3-dipolar cycloaddition due to the low polarity of the transition state [18]. Sainudeen et al. analyzed the solvent polarity of zwitterionic merocyanine using quantum chemical calculations. They found that solvents play a remarkable role in the structure and in the first hyperpolarizability of merocyanine monomers and aggregates [19]. Thus far, these attempts to elucidate the adsorption process remain at a molecular level, and most of them were carried out in vacuum or water solution conditions.

In this paper, a comprehensive analysis of the effect of solvent polarity is presented from the perspective of interactions among the solvent, the solute, and the surface. First, the electronic structure of C₁₈SH, C₁₈S, and different solvents are considered. Then, the adsorption of different solvent molecules on the Cu (111) surface is calculated to interpret the interaction between the solvent and the surface. Based on the simulation, the effect of solvent polarity on the quality of C₁₈SH SAMs on the Cu surface is explained through the proposed mechanisms. This work helps us to better understand the micro-mechanisms of solvent polarity effects of C₁₈SH on pure Cu surfaces. The method can be extended to understand interactions between other SAMs and metal surfaces.

2. Results

2.1. Electronic Structure of C₁₈SH, C₁₈S and Different Solvents

The maps of the Highest Occupied Molecular Orbital (HOMO) and the Lowest Unoccupied Molecular Orbital (LUMO) are shown in Figure 1. The quantitative results of quantum chemical parameters are as listed in Table 1.

The HOMO and LUMO regions of different molecules are mainly contributed by O, N, and S elements and the benzene ring. This indicates that these are the adsorption sites on the metal surface. As indicated in Table 1, the energy of LUMO, E_L , is greatly reduced after C₁₈SH dissociates into C₁₈S. E_L represents the electron acceptability, which is directly related to the electron affinity and characterizes the susceptibility of the molecule against attacks by nucleophiles. The lower value of E_L means stronger electron acceptability of the molecules, indicating the strong interaction between the Cu surface and C₁₈S. This is also verified through the increased fraction of electron transfer, ΔN , from the Cu surface to C₁₈S. Furthermore, it is noted that the difference in ΔN between C₁₈SH and different solvent molecules is not very high.

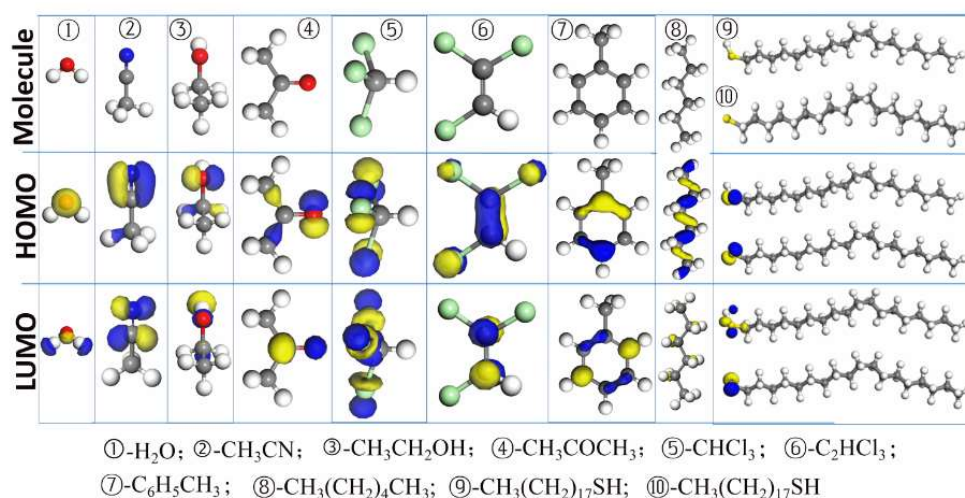


Figure 1. The map of the HOMO and LUMO for different molecules with an isovalue of ± 0.10 e.

Table 1. Quantum chemical parameters derived for different molecules at 298 K. The absolute electronegativity (χ), the global hardness (η), and the fraction of electron transfer (ΔN), were calculated by Equations (1)–(3), as described in the Materials and Methods section.

Name	Species	E_H (eV)	E_L (eV)	χ	η	ΔN
Water	H ₂ O	−0.255	0.054	0.100	0.155	14.0
Acetonitrile	CH ₃ CN	−0.299	−0.012	0.156	0.143	15.1
Ethanol	CH ₃ CH ₂ OH	−0.228	0.043	0.092	0.136	16.0
Acetone	CH ₃ COCH ₃	−0.214	−0.064	0.139	0.075	29.4
Chloroform	CH ₃ Cl ₃	−0.272	−0.078	0.175	0.097	22.6
Trichloroethylene	C ₂ HCl ₃	−0.226	−0.066	0.146	0.080	27.4
Toluene	C ₆ H ₅ CH ₃	−0.217	−0.038	0.128	0.090	24.5
<i>n</i> -hexane	CH ₃ (CH ₂) ₄ CH ₃	−0.270	0.059	0.106	0.164	13.1
<i>n</i> -octadecanethiol	C ₁₈ SH	−0.206	−0.005	0.105	0.101	21.7
Dislocated state	C ₁₈ S	−0.201	−0.186	0.194	0.007	312.7

2.2. The Adsorption for C₁₈SH, C₁₈S and Solvent Molecules on Cu Surface

The stable adsorption structures and energies of C₁₈SH and C₁₈S (the dissociated state of C₁₈SH) on the Cu (111) surface in different solvents are shown in Figures 2 and 3, where the stable adsorption energies of solvent molecules are also added and compared. The dominant effect is due to interactions between sulfur group and the Cu surface, based on the well-known hard-soft concept of Pearson.

As shown in Figure 2, H₂O adsorbs preferentially at the top site, with its molecular plane parallel to the surface. This result is consistent with a previous STM observation, which indicates an atop adsorption site [20]. Furthermore, the adsorption energy for water on a Cu surface is −0.51 eV, which is also consistent with the reported value of 0.51–0.55 eV [21], 0.54–0.57 eV [22], and 0.42 eV [23]. For the solvent molecules, elements O, N, S, and Cl are easily absorbed by the Cu atoms, because these atoms have many electrons and prefer the acidic Cu sites. Furthermore, it can be seen that only CH₃CN is vertically adsorbed to the surface; others molecules are parallel to the surface. The covered area (the dotted black line in Figure 2) for C₆H₅CH₃ and CH₃(CH₂)₄CH₃ is larger, due to their bigger molecule sizes. In order to obtain the strength of interaction between the Cu surface and different solvent molecules, the adsorption energy per unit area is plotted and compared, as shown in Figure 3. The adsorption energies are not much different for most solvent molecules and C₁₈SH; this is in accordance with previous quantum chemical parameters, as indicated in Table 1. As we know, C₁₈SH can be dissociated into C₁₈S (after losing one H atom) on the substrate surface. Therefore, the adsorption of C₁₈S is also considered in this paper [24]. As indicated in Figure 3, the adsorption

energy per unit area of $C_{18}S$ decreases from $-3.24 \text{ eV}\cdot\text{\AA}^{-2}$ to $-3.37 \text{ eV}\cdot\text{\AA}^{-2}$ in solvents with an increased dielectric constant of 1 to 78.54. Therefore, the adsorption energy per unit area for $C_{18}S$ is much smaller than that for $C_{18}SH$; this applies to the different solvent molecules as well. This indicates that $C_{18}S$ can be easily self-assembled on the Cu surface through competitive adsorption. Furthermore, the adsorption energy of $C_{18}S$ decreases in solvents with increased dielectric constant, which can well explain the previous experimental phenomenon that the $C_{18}S$ coverage on the Cu surface in the CH_3CH_2OH solution was higher than in the $CH_3(CH_2)_4CH_3$ solution at the assembly stage [13], as indicated in Figure S1.

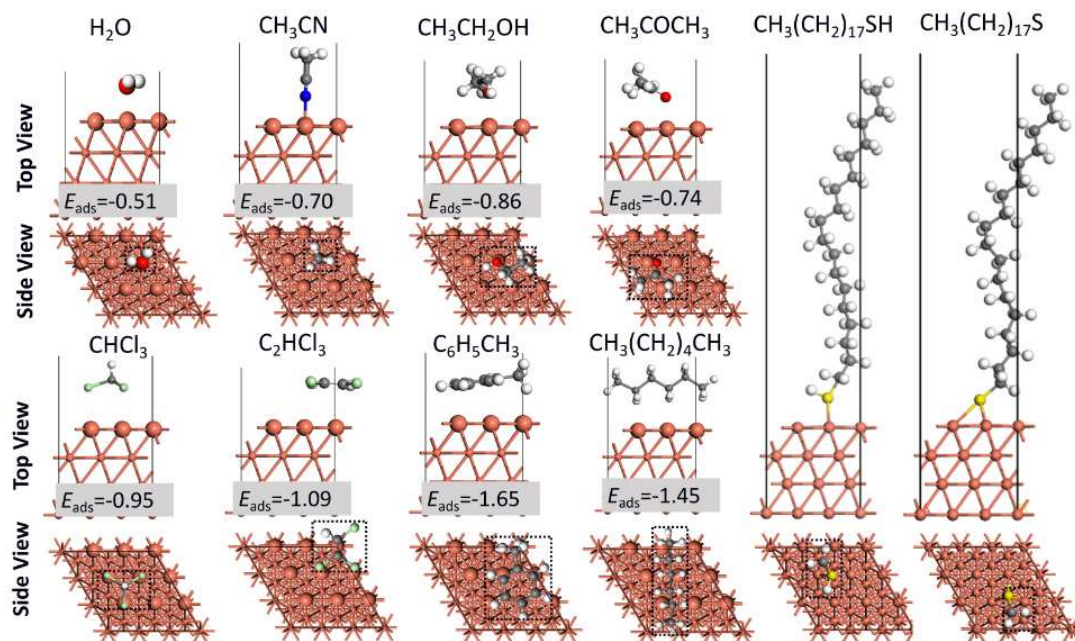


Figure 2. The adsorption structures of different solvent molecules in corresponding solvents as well as $C_{18}SH$ and $C_{18}S$ in a water solution. The unit of adsorption energy is in eV. More details are given in Table S1.

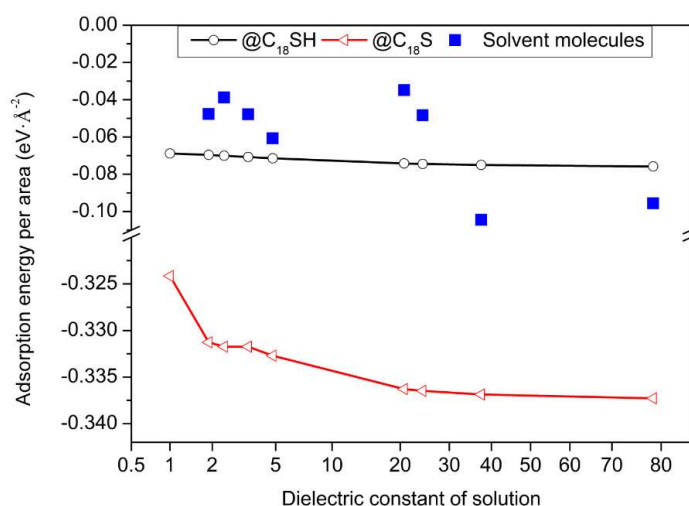


Figure 3. The adsorption energies of $C_{18}SH$, $C_{18}S$, and different solvent molecules in different solvents. The x-axis labelled for the dielectric constant of 1-Vacuum; 1.89- $CH_3(CH_2)_4CH_3$; 2.40- $C_6H_5CH_3$; 3.42- C_2HCl_3 ; 4.81- CH_3Cl_3 ; 20.7- CH_3COCH_3 ; 24.3- CH_3CH_2OH ; 37.5- CH_3CN ; 78.5- H_2O .

2.3. The Interaction between C18SH and Solvent Molecules

In order to understand the reason for the adsorption energy changes in different solvents, we compare the different energies, as shown in Figure 4.

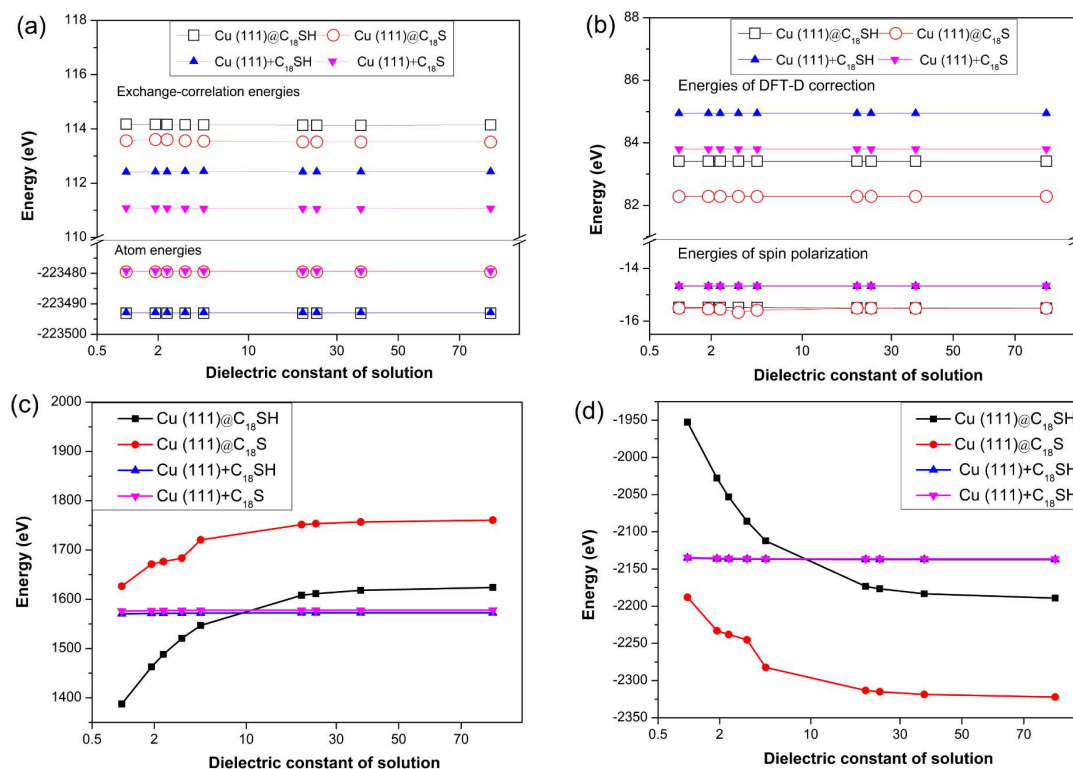


Figure 4. The energies of Cu (111) adsorption of C₁₈SH in different solvents: (a) Atom and exchange-correlation energies; (b) spin-polarization and Density Functional Theory Dispersion (DFT-D) correction energies; (c) electrostatic energies; (d) kinetic energies. The @ sign stands for the adsorption state on the facet and the + sign stands for the sum of the separate energy. The x-axis labelled for dielectric constant of 1 Vacuum; 1.89–CH₃(CH₂)₄CH₃; 2.40–C₆H₅CH₃; 3.42–C₂HCl₃; 4.81–CH₃Cl₃; 20.7–CH₃COCH₃; 24.3–CH₃CH₂OH; 37.5–CH₃CN; 78.5–H₂O.

Based on Figure 4, the atomic energy, exchange-correlation energy, spin polarization and DFT-D correction energy are not greatly changed in different solvents. The electrostatic energies gradually increase while the kinetic energies decrease with increasing dielectric constant. Furthermore, the energies are not greatly changed if we sum the corresponding energy before adsorption, illustrating that the change is caused by the interaction between Cu (111) and C₁₈SH (or C₁₈S).

As we know, the C₁₈SH is inherently non-polar and predominantly hydrophobic in nature, although the SH group provides a weakly polar character. When the C₁₈SH solute molecule is surrounded by solvent molecules with different dielectric constants, the C₁₈SH can generate a strong pull force with polar molecules and a weak compressive force with polar solvents. Although the increased polarizability of S compared to C provides a subtly greater polar character, SH groups are far less polarized than OH groups. Thus, a weak push force is generated in non-polar solvents, while a strong pull force is generated in non-polar solvents. When the C₁₈SH is absorbed on the Cu (111) surface, the electrostatic interactions on the sulfur end disappears, but the electrostatic interactions on the other position still exist. As a result, the electrostatic interaction is quickly reduced in a polar solution (higher electrostatic energy means low interaction). The force on the hydrophobic end still exists after the adsorption, and it generates both a pull force in the non-polar solvent, and a compressive force in the polar solvent. The generated push force in the polar solvent limits the mobility of C₁₈SH.

Therefore, the kinetic energies for the adsorption of $C_{18}SH$ on Cu (111) decrease with increasing dielectric constant (more polar molecules).

In order to understand the interaction between $C_{18}SH$ and solvent molecules, the radial distribution function between $C_{18}SH$ and the solvent was analyzed based on a molecular dynamics (MD) simulation, as shown in Figure 5. There is a strong peak at 1.2 Å in the $CH_3(CH_2)_4CH_3$ solution, and no obvious peak in CH_3CH_2OH solution. This indicates that there is a high probability for $CH_3(CH_2)_4CH_3$ to be distributed on the $-CH_3$ site. This confirms that the $-CH_3$ site has indeed a great interaction with $CH_3(CH_2)_4CH_3$ molecules and a weak interaction with CH_3CH_2OH molecules.

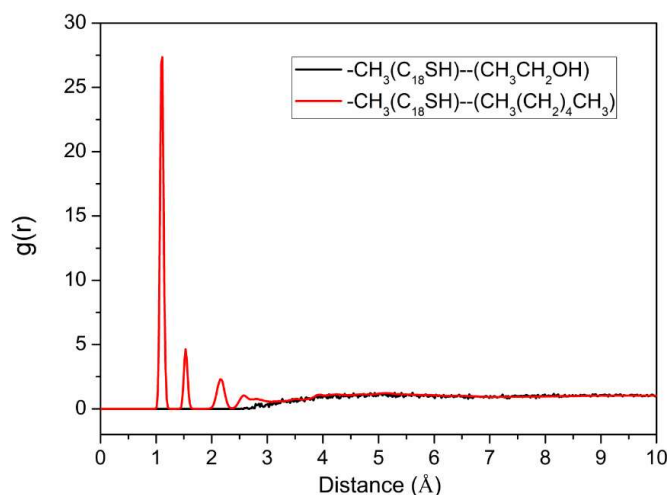


Figure 5. The radial distribution between the $-CH_3$ site of $C_{18}SH$ and solvent molecules in a 24.3- CH_3CH_2OH and 1.89- $CH_3(CH_2)_4CH_3$ solution.

3. The Effect of Solvent Polarity on the Quality of Self-Assembled $C_{18}SH$

Based on our previous results, the effect of solvent polarity on the quality of self-assembled $C_{18}SH$ on a Cu (111) plane can be illustrated in Figure 6.

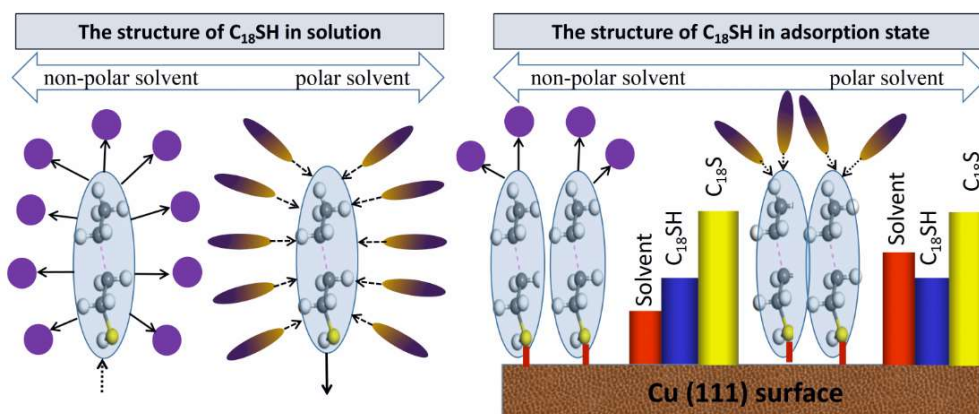


Figure 6. The adsorption of $C_{18}SH$ on the Cu (111) surface in polar and non-polar solvents, where the columnar chart represents the adsorption energies per unit area. The inward arrows present a push force, the outward arrows present a pull force, the solid line stands for a strong interaction, and the dash lines stand for a weak interaction.

As shown, the $C_{18}SH$ is embedded in the solute molecules, forming a cavity within the dielectric layer. The polarization charge distribution is determined by the generation of the charges on the cavity

surface. The polarity can generate interaction forces between the molecules of solvent and the solute. Because of the predominantly hydrophobic property of $C_{18}SH$ in nature, $C_{18}SH$ generates a strong pull force with non-polar molecules and a weak compressive force with polar solvents. The solvent polarity effect is manifested through the interaction between SAMs and solvent molecules. When the $C_{18}SH$ adsorbs on the Cu (111) surface, the interaction between the $-SH$ group and the solute disappears due to an intense chemical adsorption, while interactions between other positions of the $C_{18}SH$ and the solute still exists. The hydrophobic end mainly consists of CH groups, and it generates a great pull interaction with non-polar solvents. The generated pull interaction makes the adsorption unstable. Therefore, the kinetic energies of Cu (111) adsorbed by $C_{18}SH$ decrease along with increasing dielectric constant. A further MD simulation confirm that the $-CH_3$ site does indeed have a great interaction with $CH_3(CH_2)_4CH_3$ molecules and a weak interaction with CH_3CH_2OH molecules. The above effect significantly increases the surface coverage of $C_{18}SH$ on Cu in an ethanol solution, compared with that in an n-hexane solution at the late stabilized stage.

4. Materials and Methods

Quantum chemical calculations can provide insights into the design of inhibitor systems with superior properties and elucidate the adsorption process at a molecular level [25]. The Dmol³⁺ module of the Materials Studio software (Accelrys Inc., San Diego, CA, USA) was employed for the quantum chemistry calculations. For the calculations, the Cu (111) facet has been widely chosen as an ideal model system to investigate the structure, stability, and adsorption properties, since it is the most stable surface under realistic conditions [26]. A supercell (4×4) was built with the following dimensions: $7.75 \times 7.75 \times 6.32 \text{ \AA}^3$ (as indicated in Figure S2). The Cu (111) lattice structure was divided into four layers, and the two bottom layers were constrained. The top site (above the Cu atom of the central plane), the bridge site (between the two Cu atoms, above the contact location), the face centered cubic (fcc) site (above the triangle of the Cu atoms on the plane, or directly above a Cu atom in the next layer below the plane), and the hexagonal close packing (hcp) site (above the triangle of Cu atoms on the plane, or directly above a Cu atom in the third layer below the plane) were considered during the adsorption study. The most stable adsorption site was determined based on the minimum energy of the system.

During the calculations, the self-consistent periodic Density Functional Theory (DFT) was used to study the relative stability and reactivity of the surface species on the Cu (111) surface. The Gradient-Corrected Functionals (GGA), in the form of the Perdew-Burke-Ernzerhof (PBE) approximation to the exchange-correlation energy, and the double-numerical quality basis, which was set with Double Numerical plus Polarization (DNP) functions, were employed. The Effective Core Potential (ECP) was used to handle the core electrons of the metallic atoms. Standard Kohn-Sham Density Functional Theory Dispersion (DFT-D) correction was used for the corrective calculation of van der Waals dispersion. A thermal smearing was adopted at 0.002 hartree, with a real-space cutoff at 4.4 \AA . The k-point separation was at 0.04 \AA^{-1} . The solvent effect was considered by using a conductor-like screening model (COSMO) with different dielectric constant values [27]. The dielectric constants of water (H_2O), acetonitrile (CH_3CN), ethanol (CH_3CH_2OH), acetone (CH_3COCH_3), chloroform (CH_2Cl_3), trichloroethylene (C_2HCl_3), toluene ($C_6H_5CH_3$), n-hexane ($CH_3(CH_2)_4CH_3$) and vacuum are 78.5, 37.5, 24.3, 20.7, 4.81, 3.42, 2.40, 1.89 and 1, respectively. The calculated lattice constants of Cu was consisted with the experimental result, as indicated in Table S2.

A Molecular Dynamics (MD) simulation was carried out with 1 $C_{18}SH$ and 100 solvent molecules in an amorphous cell. A COMPASS force field was used during the optimization as indicated in Figure S3. The initial models with 3D periodic boundary conditions were optimized via the smart minimizing method until the energy gradient reaches less than 0.1 $\text{kcal}\cdot\text{mol}^{-1}$. Moreover, the operating temperature was set at 298 K and controlled by means of the Nose thermostat method to match the real experiment procedure. Then, NVT (constant molecule numbers, volume and temperature) were used for the dynamic calculation. The van der Waals interaction was calculated using an atom-based

method with a cutoff radius of 18.5 Å, while the long-range corrections were adopted outside 15 Å. The electrostatic summation method was calculated using the Ewald method with an accuracy of 10^{-5} kcal·mol⁻¹ for the computation of long-range non-bond energies in periodic systems. The details of the coordinates of atoms before C₁₈SH was adsorbed and after C₁₈SH was adsorbed on the Cu surface in vacuum are indicated in Tables S3 and S4, respectively.

Some parameters of molecular orbitals, such as absolute electronegativity (χ), the global hardness (η), and the fraction of electron transfer (ΔN), were also calculated using Equations (1)–(3).

$$\chi = (-E_H - E_L)/2 \quad (1)$$

$$\eta = (-E_H + E_L)/2 \quad (2)$$

$$\Delta N = \frac{\chi_{Cu} - \chi_{mol}}{2(\eta_{Cu} + \eta_{mol})} \quad (3)$$

where E_H and E_L are, respectively, the energies of the HOMO and the LUMO for the corresponding molecules. In order to calculate the fraction of electron transfer, a theoretical value for the absolute electronegativity of Cu is taken as 4.48 eV, and a global hardness as 0 eV·mol⁻¹, assuming the Cu atoms are softer than the neutral metallic atoms [28,29].

The interaction energy E_{ads} between the Cu (111) surface and the molecules is computed by:

$$E_{ads} = E_{total} - E_{molecule} - E_{surface} \quad (4)$$

where E_{total} is the total energy of the system in different solutions, including the energy of water molecules and the metal plane; $E_{molecule}$ is the molecules energy in different solutions; $E_{surface}$ is the energy of the metal surface in different solutions. In the current definition, the higher negative value of E_{ads} indicates a more stable adsorption on the surface [30,31].

E_{atom} (atomic energies) is obtained from atomic reference data for electronic structure calculations. The E_{elst} (Electrostatic energy), E_{kine} (kinetic energy), E_{XC} (exchange-correlation energy), E_{spin} (Spin-polarization energy), and E_{DFT-D} (DFT-D correction energy) can be calculated by Equations (5)–(9), respectively [32].

$$E_{elst} = -0.5\langle Z|D|Z \rangle - \langle \rho|D|Z \rangle - \langle \rho|D|\tilde{\rho} \rangle + 0.5\langle \tilde{\rho}|D|\tilde{\rho} \rangle \quad (5)$$

$$E_{kine} = 0.5N_f k_B T \quad (6)$$

$$E_{XC}[n] = \int n(\mathbf{r}) \varepsilon_{XC}[n(\mathbf{r})] d\mathbf{r} \quad (7)$$

$$E_{spin} = E(M_0) - E(0) \quad (8)$$

$$E_{DFT-D} = S_i \sum_{i=1}^N \sum_{j>i}^N f(S_R R_{ij}^0, R_{ij}) C_{6,ij} R_{ij}^{-6} \quad (9)$$

In the above equations, Z is the nuclear charges, $D = BA^{-1}B$, B and A are Coulomb matrices, ρ is the electron density, $\tilde{\rho}$ is the auxiliary density to solve the Poisson equation for the electrostatic potential of the solute, and N_f is the number of degrees of freedom. k_B is the Boltzmann constant, T is the absolute temperature, $n(\mathbf{r})$ is the number of the particles, $\varepsilon_{XC}[n(\mathbf{r})]$ is the exchange-correlation energy per particle in a uniform electron gas, $E(M_0)$ is the energy for the ground-state magnetic moment in the absence of an external field, and $E(0)$ is the energy when the ground-state magnetic moment is equal to zero. S_i is the XC-functional dependent factor where $S_R \neq 1$ and $S_6 \equiv 1$, $f(S_R R_{ij}^0, R_{ij})$ is the damping function to express short range $S_R R_{ij}^0$ by long-range R_{ij} . $C_{6,ij} R_{ij}^{-6}$ is a long range isotropic potential.

5. Conclusions

Based on the previous experimental findings, solvent polarity plays an important role in the adsorption of C₁₈SH SAMs on Cu surfaces. The effect of solvent polarity on the quality of self-assembled C₁₈SH on Cu (111) surfaces has been systematically analyzed using first-principles calculations. The results have revealed the molecular mechanisms behind the effect of solvent polarity.

C₁₈SH is inherently non-polar and predominantly hydrophobic in nature, although the SH group provides a weakly polar character. In a non-polar molecule solution, there is a great pull interaction between C₁₈SH and non-polar molecules. However, in a polar molecule solution, there is a weak interaction between C₁₈SH and polar molecules. Due to the great interaction between C₁₈S and the Cu surface, C₁₈SH can self-assemble on the Cu surface ($E_{\text{ads}} = -3.37$ eV and $\Delta N = 312.7$). After this, the electrostatic interactions on the sulfur end disappears, but the electrostatic interactions on the other positions still exist. The adsorption energy decreases greatly with increasing dielectric constant (or polarity). This is mainly caused by the change of electrostatic energies and kinetic energies in different solutions, attributable to the different types of interaction. The electrostatic interaction is quickly reduced in polar solutions due to the disappearance of electrostatic interactions on the sulfur end, and the reduced kinetic energies are due to the solvophobic cage-type effects which limit the mobility of C₁₈SH. A further MD simulation also verifies that the -CH₃ site has indeed a strong interaction with CH₃(CH₂)₄CH₃ molecules and a weak interaction with CH₃CH₂OH molecules. This study helps us to better understand the micro-mechanisms of solvent polarity effects for C₁₈SH adsorption on Cu surfaces.

Supplementary Materials: The following is available online. Figure S1: Impedance plots of C18SH SAMs on Cu surfaces in different solvents in 0.1 mol·L⁻¹ KCl as the supporting electrolyte. Figure S2: Top and side view of the Cu (111) surface. Figure S3: MD model in different solutions. Table S1: Stable adsorption energies of different species on the Cu (111) surface. Table S2: The calculated lattice constants of Cu, as compared with experimental results of reference. Table S3: The coordinates of atoms on a Cu (111) surface after the optimization in vacuum conditions. Table S4: The coordinates of atoms when C₁₈SH is adsorbed on the top site of the Cu (111) surface after the optimization in vacuum conditions.

Acknowledgments: The financial support from the National Natural Science Foundation of China (No. 21676216), the China Postdoctoral Science Foundation (No. 2014M550507; 2015T81046), and the Innovative Projects of Northwest University (YZZ17140) are greatly acknowledged. This research project was supported by the Centre for High Performance Computing of Northwestern Polytechnical University, China.

Author Contributions: J.H. and Z.C. conceived and designed the calculations; S.H. performed the calculations; Y.Z. and L.Z. analyzed the data; H.M. contributed analysis tools; J.H. wrote the paper with input from Z.C.

Conflicts of Interest: The authors declare no conflicts of interest.

References

1. Hosseinpour, S.M.; Forslund, C.M.; Johnson, J.; Leygraf, P.C. Atmospheric corrosion of Cu, Zn, and Cu–Zn alloys protected by self-assembled monolayers of alkanethiols. *Surf. Sci.* **2016**, *648*, 170–176. [[CrossRef](#)]
2. Shi, M.; Hong, Q.L.; Nian, B.L. Study on the influences of two thiazole flavor ingredients on Cu corrosion caused by chloride ion. *J. Colloid Interface Sci.* **2017**, *505*, 929–939.
3. Bi, H.; Burstein, G.T.; Rodriguez, B.B.; Kawaley, G. Some aspects of the role of inhibitors in the corrosion of copper in tap water as observed by cyclic voltammetry. *Corros. Sci.* **2016**, *102*, 510–516. [[CrossRef](#)]
4. Wang, Y.; Hu, J.; Wang, Y.; Yu, L. A new method for preventing corrosion failure: Thiourea and Hexamethylenetetramine as inhibitor for copper. *Bull. Korean Chem. Soc.* **2016**, *37*, 1797–1811. [[CrossRef](#)]
5. Love, J.C.; Estroff, L.A.; Kriebel, J.K.; Nuzzo, R.G.; Whitesides, G.M. Self-assembled monolayers of Thiolates on metals as a form of nanotechnology. *Chem. Rev.* **2005**, *105*, 1103–1169. [[CrossRef](#)] [[PubMed](#)]
6. Nozomi, S.; Masahiko, Y. Synthesis and self-Assembly of chiral cylindrical molecular complexes: Functional heterogeneous liquid-solid materials formed by helicene oligomers. *Molecules* **2018**, *23*, 277.
7. Calbo, J.; Sancho-García, J.C.; Ortí, E.; Aragón, J. Quantum-Chemical Insights into the Self-Assembly of Carbon-Based Supramolecular Complexes. *Molecules* **2018**, *23*, 118. [[CrossRef](#)] [[PubMed](#)]

8. Park, C.S.; Lee, H.J.; Lee, D.; Jamison, A.C.; Galstyan, E.; Wosik, W.Z.; Freyhardt, H.C.; Jacobson, A.J.; Lee, T.R. Semifluorinated alkylphosphonic acids form high-Quality self-Assembled monolayers on Ag-coated yttrium barium copper oxide tapes and enable filamentization of the tapes by microcontact printing. *Langmuir* **2016**, *32*, 8623–8630. [[CrossRef](#)] [[PubMed](#)]
9. Bain, C.D.; Troughton, E.B.; Tao, Y.T.; Evall, J.; Whitesides, G.M.; Nuzzo, R.G. Formation of monolayer films by the spontaneous assembly of organic thiols from solvent onto gold. *J. Am. Chem. Soc.* **1989**, *111*, 321–335. [[CrossRef](#)]
10. Dai, J.Y.; Li, Z.G.; Jin, J.; Cheng, J.J.; Kong, J.; Bi, S.P. Study of the solvent effect on the quality of dodecanethiol self-assembled monolayers on polycrystalline gold. *J. Electroanal. Chem.* **2008**, *624*, 315–322. [[CrossRef](#)]
11. Sur, U.K.; Lakshminarayanan, V. Effect of bulk structure of some non-aqueous solvents on the barrier properties of alkanethiol monolayer. *J. Electroanal. Chem.* **2001**, *516*, 31–38. [[CrossRef](#)]
12. Sur, U.K.; Lakshminarayanan, V. A study of the hydrophobic properties of alkanethiol self-assembled monolayers prepared in different solvents. *J. Electroanal. Chem.* **2004**, *565*, 343–350. [[CrossRef](#)]
13. Zhang, Y.Z.; Zhou, J.; Zhang, X.; Hu, J.; Gao, H. Solvent polarity effect on quality of n-octadecanethiol self-assembled monolayers on copper and oxidized copper. *Appl. Surf. Sci.* **2014**, *320*, 200–206. [[CrossRef](#)]
14. El-Kareh, L.; Mehring, P.; Caciuc, V.; Atodiresei, N.; Beimborn, A.; Blügel, S.; Westphal, C. Self-assembled monolayers of methylselenolate on the Au (111) surface: A combined STM and DFT study. *Surf. Sci.* **2014**, *619*, 67–70. [[CrossRef](#)]
15. Castejón, H.J.; Bernecker, C.R. Modeling the liquid–gas interface using self-assembled monolayers. *Surf. Sci.* **2012**, *606*, 1274–1279. [[CrossRef](#)]
16. Milan, R.; Anna, R.; Ria, B. Theoretical Study of Molecular Structure and Physicochemical Properties of Novel Factor Xa Inhibitors and Dual Factor Xa and Factor IIa Inhibitors. *Molecules* **2016**, *21*, 185.
17. Breitwieser, R.; Campiglio, P.; Chacon, C.; Repain, V.; Nemausat, R.; Girard, Y.; Lagoute, J.; Rousset, S. Variable temperature STM study of Co deposition on a dodecanethiol self assembled monolayer. *Surf. Sci.* **2012**, *606*, 542–548. [[CrossRef](#)]
18. Benchouk, W.; Mekelleche, S.M.; Silvi, B.; Aurell, M.J.; Domingo, L.R. Understanding the kinetic solvent effects on the 1,3-dipolar cycloaddition of benzonitrile N-oxide: A DFT study. *J. Phys. Org. Chem.* **2011**, *24*, 611–618. [[CrossRef](#)]
19. Sainudeen, Z.H.; Ray, P.C. Nonlinear optical properties of zwitterionic merocyanine aggregates: role of intermolecular interaction and solvent polarity. *J. Phys. Chem. A* **2005**, *109*, 9095–9103. [[CrossRef](#)] [[PubMed](#)]
20. Fomin, E.; Tatar khanov, M.; Mitsui, T.; Rose, M.; Ogletree, D.F.; Salmeron, M. Vibrationally assisted diffusion of H₂O and D₂O on Pd (111). *Surf. Sci.* **2006**, *600*, 542–546. [[CrossRef](#)]
21. Ren, J.; Meng, S. Atomic Structure and Bonding of Water Overlayer on Cu (110): The Borderline for Intact and Dissociative Adsorption. *J. Am. Chem. Soc.* **2006**, *128*, 9282–9283. [[CrossRef](#)] [[PubMed](#)]
22. Schiros, T.; Haq, S.; Ogasawara, H.; Takahashi, O.; Öström, H.; Andersson, K.; Pettersson, L.G.M.; Hodgson, A.; Nilsson, A. Structure of water adsorbed on the open Cu (110) surface: H-up, H-down, or both? *Chem. Phys. Lett.* **2006**, *429*, 415–419. [[CrossRef](#)]
23. Chen, L.; Zhang, Q.; Zhang, Y.; Li, W.Z.; Han, B.; Zhou, C.; Wu, J.; Forrey, R.C.; Garg, D.; Cheng, H. A first principles study of water dissociation on small copper clusters. *Phys. Chem. Chem. Phys.* **2010**, *12*, 9845–9851. [[CrossRef](#)] [[PubMed](#)]
24. Cometto, F.P.; Paredes-Olivera, P.; Macagno, V.A.; Patrio, E.M. Density functional theory study of the adsorption of alkanethiols on Cu (111), Ag (111), and Au (111) in the low and high coverage regimes. *J. Phys. Chem. B* **2005**, *109*, 21737–21748. [[CrossRef](#)] [[PubMed](#)]
25. Chatterjee, A.; Iwasaki, T.; Ebina, T.; Hayashi, H. Quantum chemical calculation on clay-water interface. *Appl. Surf. Sci.* **1997**, *12*, 167–170. [[CrossRef](#)]
26. Zuo, Z.J.; Wang, L.; Han, P.D.; Huang, W. Insights into the reaction mechanisms of methanol decomposition, methanol oxidation and steam reforming of methanol on Cu (111): A density functional theory study. *Int. J. Hydrogen Energ.* **2014**, *39*, 1664–1679. [[CrossRef](#)]
27. Diley, B. The conductor-like screening model for polymers and surfaces. *Mol. Simul.* **2006**, *32*, 117–123. [[CrossRef](#)]
28. Sastri, V.; Perumareddi, J. Molecular orbital theoretical studies of some organic corrosion inhibitors. *Corrosion Houston TX* **1997**, *53*, 617–622. [[CrossRef](#)]

29. Pearson, R.G. Absolute electronegativity and hardness: Application to inorganic chemistry. *Inorg. Chem.* **1988**, *27*, 734–740. [[CrossRef](#)]
30. Hu, J.; Zhao, X.; Chen, W.; Su, H.; Chen, Z. Theoretical insight into the mechanism of photoelectrochemical oxygen evolution reaction on BiVO₄ anode with oxygen vacancy. *J. Phys. Chem. C* **2017**, *121*, 18702–18709. [[CrossRef](#)]
31. Huang, Z.Q.; Long, B.; Chang, C.R. A theoretical study on the catalytic role of water in methanol steam reforming on PdZn (111). *Catal. Sci. Technol.* **2015**, *5*, 2935–2944. [[CrossRef](#)]
32. Delley, B. From molecules to solids with the DMol3 approach. *J. Chem. Phys.* **2000**, *113*, 7756–7764. [[CrossRef](#)]

Sample Availability: Samples of the compounds are not available from the authors (this is a computational work).



© 2018 by the authors. Licensee MDPI, Basel, Switzerland. This article is an open access article distributed under the terms and conditions of the Creative Commons Attribution (CC BY) license (<http://creativecommons.org/licenses/by/4.0/>).